International Journal of Heat and Mass Transfer 150 (2020) 119346

Contents lists available at ScienceDirect

International Journal of Heat and Mass Transfer

journal homepage: www.elsevier.com/locate/hmt

Thermal routing via near-field radiative heat transfer

Jinlin Song[a], Lu Lu[a], Bowen Li[a], Bo Zhang[a], Run Hu[a,*], Xinping Zhou[b], Qiang Cheng[a,*]

[a] State Key Laboratory of Coal Combustion, School of Energy and Power Engineering, Huazhong University of Science and Technology, Wuhan 430074, China
[b] Department of Mechanics, Huazhong University of Science and Technology, Wuhan 430074, Hubei, China

ARTICLE INFO

Article history:
Received 19 September 2019
Revised 23 December 2019
Accepted 8 January 2020
Available online 17 January 2020

Keywords:
Near-field radiative heat transfer
thermal routing
many-body systems
core-shell nanoparticles
graphene

ABSTRACT

The diffusive nature of heat flow lays a formidable obstacle for directional heat manipulation, not akin to the wave-governed electromagnetics that can be well controlled in intensity and direction. By modulating the near-field radiative heat transfer among graphene/SiC core-shell (GSCS) nanoparticles, we propose the concept of thermal routing to address the directional heat manipulation in a particular many-body setup. The graphene shell introduces a minor polarizability peak and remarkably modifies the localized surface resonance of the particle, which plays a significant role in the radiative heat transfer within the many-body system consisting of GSCS nanoparticles. Consequently, Fermi levels of graphene shells matching allows directional radiative heat flow, thus enabling thermal routing manifested by variant designated temperature distributions. The proposed thermal routing could be used to dynamically tune heat flow in integrated nano-objects for thermal manipulation, and also opens avenues for exploiting novel thermal functionalities via radiative heat transfer at the nanoscale.

1. Introduction

Due to its diffusive nature, heat flow has long been considered impossible or at least formidable to manipulate, whose Laplacian-type governing equations intrinsically differ from the parabolic wave equations, resulting in the nearly impossibility to borrow the wave-related technologies and strategies for heat flow control. More than that, almost all energy will be converted into low-grade heat energy eventually more or less, so thermal issues almost arise from everywhere, especially in the microscale electronics and photoelectronics, at which the disordered dissipation of heat becomes a crucial bottleneck for the working performance maintenance and further improvement. Hence, the ordered heat transfer is more desirable in thermal manipulation. For example, controllable direction of heat flow can prevent heat-sensitive components overheating under the premise of maintaining the heat flux. Thus exploring alternative feasibility of heat flow manipulation against its diffusive nature never stops and draws increasing attentions recently at the nanoscale [1–7]. Several prototypes of phononic thermal transistor, logic gates as well as thermal memories, have been put forward in order to process heat currents for various functionalities [8–10]. However, in contrast to phonon, photon possesses higher propagating speed and avoids intrinsic Kapitza resistances of phonon mediated devices which make it have great potential for faster and higher-efficiency processing and managing heat currents [11]. It is well known that, photon mediated heat transfer at the nanoscale, *i.e.*, near-field radiative heat transfer (NFRHT), governed by the evanescent waves, can exceed the Planck's prediction by several orders of magnitude [12–19]. Therefore, utilizing the NFRHT is a feasible way to manipulate heat currents when the dimension of elementary devices reduces to nanoscale. Based on NFRHT, a photon-mediated transistor was theoretically suggested to realize the switching, modulation and amplification of heat currents [20–24]. Many other important developments have been carried out in recent years, such as near-field thermal rectifier and active thermal switching [25,26], but most of these works focus on the manipulation of intensity of heat flux rather than direction.

Graphene, consisting of a monolayer of carbon atoms in a two-dimensional honeycomb lattice, has attracted extensive attention because of its unique optoelectronic properties [27–30]. In terms of NFRHT, graphene is frequently used to manipulate near-field heat flux by altering its surface plasmons in the mid-infrared range [31–33]. Graphene/SiC core-shell (GSCS) nanoparticles, which can be fabricated by using thermal decomposition of graphene to SiC nanoparticles, possess additional propagating modes of electromagnetic waves induced by graphene shells [34,35]. Meanwhile, they have tunable optical properties when electrically biased, for example, applying an external bias by electrical wires using measuring nanoscale Casimir force in the plane-sphere geometry for references [36–38], or utilizing distant gates far from the particle

* Corresponding authors.
E-mail addresses: hurun@hust.edu.cn (R. Hu), chengqiang@mail.hust.edu.cn (Q. Cheng).

https://doi.org/10.1016/j.ijheatmasstransfer.2020.119346
0017-9310/

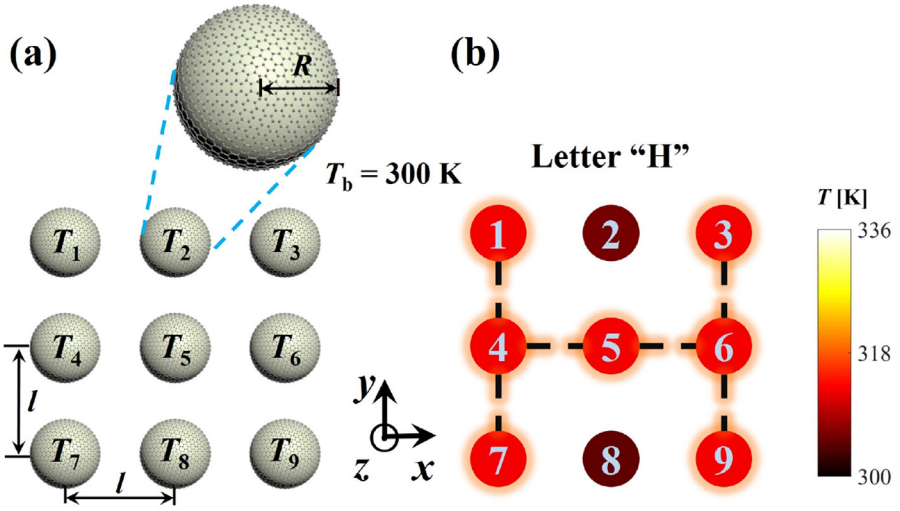

Fig. 1. (a) Diagram of the many-body system consisting of nine GSCS nanoparticles arranged in an evenly spaced 3 × 3 matrix. (b) If the distribution of Fermi levels of particles is designated, propagation path (dotted line) of heat flow among these particles can be controlled. For instance, the left-top particle is heated up to T_1 ($> T_{i\neq 1}$), and then in tens of milliseconds ($\sim 1\times10^{-2}$ s), these particles thermalize to different temperatures, and the system exhibits a designated temperature distribution, *e.g.*, the letter H (a simplified pseudo-color thermal pattern).

region which should not affect the heat transfer as mentioned in [39]. However, how do the optical properties of GSCS nanoparticles accompanied with the change of physical mechanisms affect NFRHT still remains an open question. Moreover, many-body problems are more general than two-body problems and indispensable to construct theoretical frameworks for many branches of physics. Therefore, in this work, on the basis of many-body radiative heat transfer theory [40], we theoretically investigate the near-field radiation dynamics in networks of GSCS nanoparticles, and demonstrate the thermal routing at the nanoscale via radiative heat transfer thanks to the heat flux splitting effect. We find that the modification of near-field interactions induced by graphene shells also plays an important role in radiative heat transfer. This study could be used to dynamically tune heat flow in integrated nano-objects, and opens avenues for exploiting new functionalities via radiative heat transfer at the nanoscale.

2. Theoretical model

We consider a many-body system, consisting of nine GSCS nanoparticles arranged in a 3 × 3 matrix, as sketched in Fig. 1(a). These particles, with temperatures T_i, positions p_i and polarizability tensors $\hat{\alpha}_i$, are immersed in a thermal bath at a constant temperature T_b, in which $i = 1, 2,..., N$ ($N = 9$) identifies each GSCS nanoparticle. In particular, all particles can be grafted at the end of elongated microscope tips which can apply electric bias and conductive heat flux to each one particle. Here, we investigate the temporal evolution of temperatures of particles in such a many-body system, and find that by designing the distribution of Fermi levels of particles, propagation path of heat flow among these particles can be controlled, which enables the system to show different temperature distributions. A simplified pseudo-color thermal pattern formed by the proposed system at a certain time, *i.e.*, the letter H, is schematically depicted in Fig. 1(b).

For simplicity, we assume here that all GSCS nanoparticles are much smaller than the thermal wavelength $\lambda_c = \hbar c/k_B T$ (c is the vacuum light velocity, $\hbar$ is the reduced Planck's constant, and k_B is Boltzmann's constant), so that they can be treated as radiating electric dipoles, and their electric polarizabilities can be described by the local-response approximation [41]. On the basis of the fluctuation dissipation theorem using electric dipole moments (the contribution of magnetic moments can be neglected in the thermalization process due to their small sizes [42]), the total radiation power dissipated in the ith particle reads [43]

$$\mathcal{P}_i = \mathcal{F}_i + \sum_{j\neq i}\mathcal{F}_{i,j} + \sum_{jj'}\mathcal{F}^b_{i,jj'}, \tag{1}$$

$$\mathcal{F}_i = \mathrm{Im}\int_0^\infty \frac{d\omega}{\pi}\Theta(\omega,T_i)\mathrm{Tr}\left[\hat{\mathrm{A}}_{ii}\mathrm{Im}\left(\hat{\chi}_i\right)\hat{\mathrm{C}}^\dagger_{ii}\right], \tag{2}$$

$$\mathcal{F}_{i,j} = \mathrm{Im}\int_0^\infty \frac{d\omega}{\pi}\Theta\left(\omega,T_j\right)\mathrm{Tr}\left[\hat{\mathrm{A}}_{ij}\mathrm{Im}\left(\hat{\chi}_j\right)\hat{\mathrm{C}}^\dagger_{ij}\right], \tag{3}$$

$$\mathcal{F}^b_{i,jj'} = \mathrm{Im}\int_0^\infty \frac{d\omega}{\pi}\Theta(\omega,T_b)\mathrm{Tr}\left[\hat{\mathrm{B}}_{ij}\mathrm{Im}\left(\hat{\mathrm{G}}_{jj'}\right)\hat{\mathrm{D}}^\dagger_{ij'}\right], \tag{4}$$

where $\mathcal{F}_i$ stands for the radiative cooling of the ith particle due to its self-emission in presence of other particles, $\mathcal{F}_{i,j}$ denotes the radiative heating of the ith particle by the jth one ($j \neq i$) considering the direct and indirect radiative energy among these particles, and $\mathcal{F}^b_{i,jj'}$ is the absorbed power in the ith particle from the thermal bath. $\Theta(\omega,T) = \hbar\omega[1 + 2n(\omega,T)]/2$ and $n(\omega,T)$ represents the Bose–Einstein energy distribution as a function of frequency ω and temperature T. The susceptibility tensor of the ith nanoparticle with polarizability tensor $\hat{\alpha}_i$ to describe dipolar fluctuation in the fluctuation-dissipation theorem reads $\hat{\chi}_i = \hat{\alpha}_i + k^2\hat{\alpha}_i\hat{\mathrm{G}}^\dagger_0\hat{\alpha}^\dagger_i$, where $\hat{\mathrm{G}}_0 = i\frac{k}{6\pi}\hat{1}$, $k = \omega/c$ and $\hat{1}$ is a 3 × 3 unit dyadic tensor. The elements of the free space Green tensor $\hat{\mathrm{G}}$ in this system read $\hat{\mathrm{G}}_{i\neq j} = \frac{\exp(ikr_{ij})}{4\pi r_{ij}} \times \left[\left(1 + \frac{ikr_{ij}-1}{k^2r^2_{ij}}\right)\hat{1} + \frac{3-3ikr_{ij}-k^2r^2_{ij}}{k^2r^2_{ij}}\hat{\mathbf{r}}_{ij}\otimes\hat{\mathbf{r}}_{ij}\right]$ with the unit vector $\hat{\mathbf{r}}_{ij} \equiv \mathbf{r}_{ij}/r_{ij}$ linking the centers of the ith and jth particles, where r_{ij} is the modulus of $\mathbf{r}_{ij}$. Here, $\hat{\mathrm{G}}_{ij} = \hat{\mathrm{G}}_{ji}$. The coupling matrixes $\hat{\mathrm{A}}$, $\hat{\mathrm{B}}$, $\hat{\mathrm{C}}$ and $\hat{\mathrm{D}}$ which consider the electric responses of GSCS nanoparticles and many-body interaction can be obtained from Nikbakht [44]. Note that, the contribution of higher multipoles can also be ignored because they participate to the heat transfer only at very short distances (for example, $l/R < 2.5$) [45].

The electric polarizability tensor of the i-th GSCS nanoparticle can be expressed by the following modified Clausius–Mossotti form where the graphene shell behaves as a conductive sheet with negligible thickness, and this approximation can be validated by the classical Mie theory [41,46],

$$\hat{\alpha}_i = 4\pi R_i^3\frac{\varepsilon(\omega)-\varepsilon_h+2g_i(\omega)}{\varepsilon(\omega)+2\varepsilon_h+2g_i(\omega)}\hat{1}, \tag{5}$$

in which, $\varepsilon(\omega)$ is the dielectric function of SiC which can be described by the Lorentz model [47], $\varepsilon_h = 1$ in this work denotes that the particles are immersed in vacuum, and $g_i(\omega) = \frac{i\sigma(\omega)}{\varepsilon_0 \omega R_i}$ is a dimensionless parameter considering the influence of the graphene shell on the SiC core where R_i is the radius of core and ε_0 is the vacuum permittivity. $\sigma(\omega)$ is the surface conductivity of graphene, and modeled as a sum of an intraband term and an interband term, $\sigma(\omega) = \sigma_{\text{intra}}(\omega) + \sigma_{\text{inter}}(\omega)$, and given as follows [48],

$$\sigma_{\text{intra}}(\omega) = \frac{i}{\omega + i/\tau_g} \frac{2e^2 k_B T_g}{\pi \hbar^2} \ln\left[2\cosh\left(\frac{\mu}{2k_B T_g}\right)\right], \tag{6}$$

$$\sigma_{\text{inter}}(\omega) = \frac{e^2}{4\hbar}\left[G(\hbar\omega/2) + \frac{4i\hbar\omega}{\pi}\int_0^\infty \frac{G(\xi) - G(\hbar\omega/2)}{(\hbar\omega)^2 - 4\xi^2} d\xi\right], \tag{7}$$

where $G(\xi) = \frac{\sinh(\xi/k_B T_g)}{\cosh(\mu/k_B T_g) + \cosh(\xi/k_B T_g)}$, e is the electron charge, μ is the Fermi level, $\tau_g = 1 \times 10^{-13}$ s is the relaxation scattering time, and the temperature of graphene $T_g = 300$ K is fixed in this work which has little influence on the polarizability of GSCS nanoparticles. Taking radiative correction into consideration, the dressed polarizability is given by Albaladejo et al. [49]

$$\hat{\alpha}_i = \hat{\alpha}_i^{(0)}\left\{\hat{1} - i\frac{k^3}{6\pi}\hat{\alpha}_i^{(0)}\right\}^{-1}. \tag{8}$$

In order to obtain the temporal evolution of temperatures of GSCS nanoparticles, we utilize the framework for thermal dynamics of temperatures considering the nonlinear coupled many-body system, which reads $c_i m_i \frac{\partial T_i}{\partial t} = \mathcal{P}_i$ with c_i and m_i being the specific heat capacity and mass of the ith particle. In this work, assuming that the heat capacities of nanometer-sized core and shell, *i.e.*, C_{core} and C_{shell}, are equal to those of the corresponding bulks, and the effect of the interface is neglected so that the atoms located at the interface act like volumetric atoms. Under these assumtions, the approximate specific heat capacity of ith GSCS nanoparticle can be expressed as $c_i \approx (m_{\text{core}} C_{\text{core}} + m_{\text{shell}} C_{\text{shell}})/m_{\text{i}}$ where m_{core} and m_{shell} are masses of the core and shell [50]. The temperature-dependent heat capacity of SiC core can be obtained from the work [51], and the heat capacity of graphene is identical to that of graphite above 100 K [52].

3. Results and discussion

To start with, all particles are at 300 K with the thermal bath maintaining $T_b = 300$ K hereafter. Then, only the left-top particle, *i.e.*, particle 1, is heated up to $T_1 = 400$ K by using optical pump. Then, we stop heating and let particle 1 spontaneously dissipate heat in the system, accompanied by thermalization of other particles. In this process, different particles receive different heat fluxes due to the geometric configuration of the system and Fermi level matching among particles, which give rise to different temperature distributions. We only consider $l/R \geq 3$ to ensure that the electric dipolar approximation is valid [53,54]. Fig. 2(a)–(d) shows the temperatures of nine GSCS particles as a function of time with the time interval of $\Delta t = 10^{-4}$ s in four scenarios, namely the formation of letters H, U, S and T. In Fig. 2(a), the Fermi levels of particles 2 and 8 are 0.1 eV with those of the others being 0.7 eV. Note that, Fermi levels of 0.1 and 0.7 eV are chosen due to the high splitting ratio as reported in our previous work [55]. With the increase of time, particles except particle 1 (thermal source) are heated up. However, for particles 4 and 5 which are closer and have matched Fermi levels with particle 1, their temperatures remarkably rise in a short time, and then gradually drop. When $t = 1 \times 10^{-2}$ s, temperatures of particles with Fermi levels of 0.7 eV approach nearly 313 K, while temperatures of particles 2 and 8 with Fermi levels of 0.1 eV are nearly 306 K. Hence, at $t = 1 \times 10^{-2}$ s, according to the temperature values, the hotter particles (light red) and colder ones (dark red) show an H-shaped distribution with a temperature difference of $\Delta T \approx 7$ K. The formation process of the pseudo-color thermal pattern of letter H is shown in Fig. 3, which gives the simplified pseudo-color patterns at three time points: $t = 1 \times 10^{-3}$ s, $t = 2 \times 10^{-3}$ s and $t = 1 \times 10^{-2}$ s, respectively. As we can see, radiative heat flows along with the designated H-shaped path according to the distribution of Fermi levels. At $t = 2 \times 10^{-3}$, the system still shows a out-of-order state. With the further increase of t, all temperatures will reach a similar point (≈ 310 K which takes about 3.9×10^{-2} s in this system) and then drops to $T_b = 300$ K eventually with the temperature difference finally vanishing. This situation takes time far beyond $t = 1 \times 10^{-2}$ s which is not shown here [43]. In addition, if the thermal source becomes another particle, *e.g.*, particle 5, the heat transfer is enhanced which results in a larger temperature difference with $\Delta T = 13$ K at $t = 1 \times 10^{-2}$ s, as shown in Fig. 4. In this scenario, all particles start at 300 K except particle 5 (thermal source). Then, particle 5 heats up the others and spontaneously dissipates heat in the system simultaneously. In this process, temperatures of the others with $\mu_i = 0.7$ eV increase and then gradually drop. Due to the symmetrical distribution of Fermi levels and geometry, temperatures of particles at the vertices (particles 1, 3, 7 and 9) overlap with each other, and this phenomenon also occurs for particles 4 and 6, as well as particles 2 and 8. Compared to the situation where particle 1 is the thermal source, changing particle 5 to the thermal source enhances the radiative heat transfer which leads to a larger temperature difference with $\Delta T \approx 13$ K at $t = 1 \times 10^{-2}$ s. This enables the infrared thermal pattern to have a higher contrast ratio.

Furthermore, we set $\mu_2 = \mu_5 = 0.1$ eV with Fermi levels of the others being 0.7 eV. We find that, particles 2 and 5 thermalize evidently slowly, and when $t = 1 \times 10^{-2}$ s, these nine particles show an U-shaped pattern with particles 2 and 5 at about 306 K and others at above 313 K, as shown in Fig. 2(b). Additionally, in Fig. 2(c), when $\mu_4 = \mu_6 = 0.1$ eV with the others being 0.7 eV, these nine particles show an S-shaped pattern as shown in Fig. 2(c). In Fig. 2(d), Fermi levels of four particles, *i.e.*, particles 4, 6, 7 and 9, are fixed at 0.1 eV. This designated Fermi level distribution enables the networks to show a T-shaped pattern when $t = 1 \times 10^{-2}$ s. Results also show that, the quantity of particles with non-matching Fermi levels with the thermal source, affects the temperature difference ΔT at a certain time. For instance, in Fig. 2(d), such a system exhibits a temperature difference $\Delta T > 12$ K while $\Delta T \approx 7$ K in Fig. 2(a)–(c) when $t = 1 \times 10^{-2}$ s.

A natural question comes up, *i.e.*, why the directional heat flow is formed. First, it is necessary to show the polarizability of a GSCS particle α with variant μ, as illustrated in Fig. 5(a). The major and minor polarizability peaks (several orders of magnitude less than the major ones) for $\mu = 0.1$ and 0.7 eV are marked. For a GSCS particle with $\mu = 0.1$ eV, its polarizability exhibits a major peak due to the localized surface resonance at $\omega_{sr} = 1.77 \times 10^{14}$ rad/s and a less pronounced peak located at 0.58×10^{14} rad/s. For a larger μ, the major peak almost linearly moves to a higher frequency but the minor one shows a concave increase. When $\mu =$ 0.7 eV, the major peak and minor peak are located at 2.34×10^{14} and 1.27×10^{14} rad/s. The dashed black line denotes the localized surface resonance frequency of a bare SiC nanoparticle with $R = 50$ nm corresponding to $\varepsilon_{sr} = -2$. It shows that, the graphene shell introduces a minor polarizability peak and remarkably modifies the localized surface resonance (frequency and intensity) of the particle, which plays a significant role in the radiative heat transfer in the system. Fig. 5(b) gives the polarizabilities of bare graphene shells with $R = 50$ nm under variant Fermi levels. It is seen that, the polarizability shows a pronounced peak (corresponding to the introduced minor polarizability peak of the GSCS

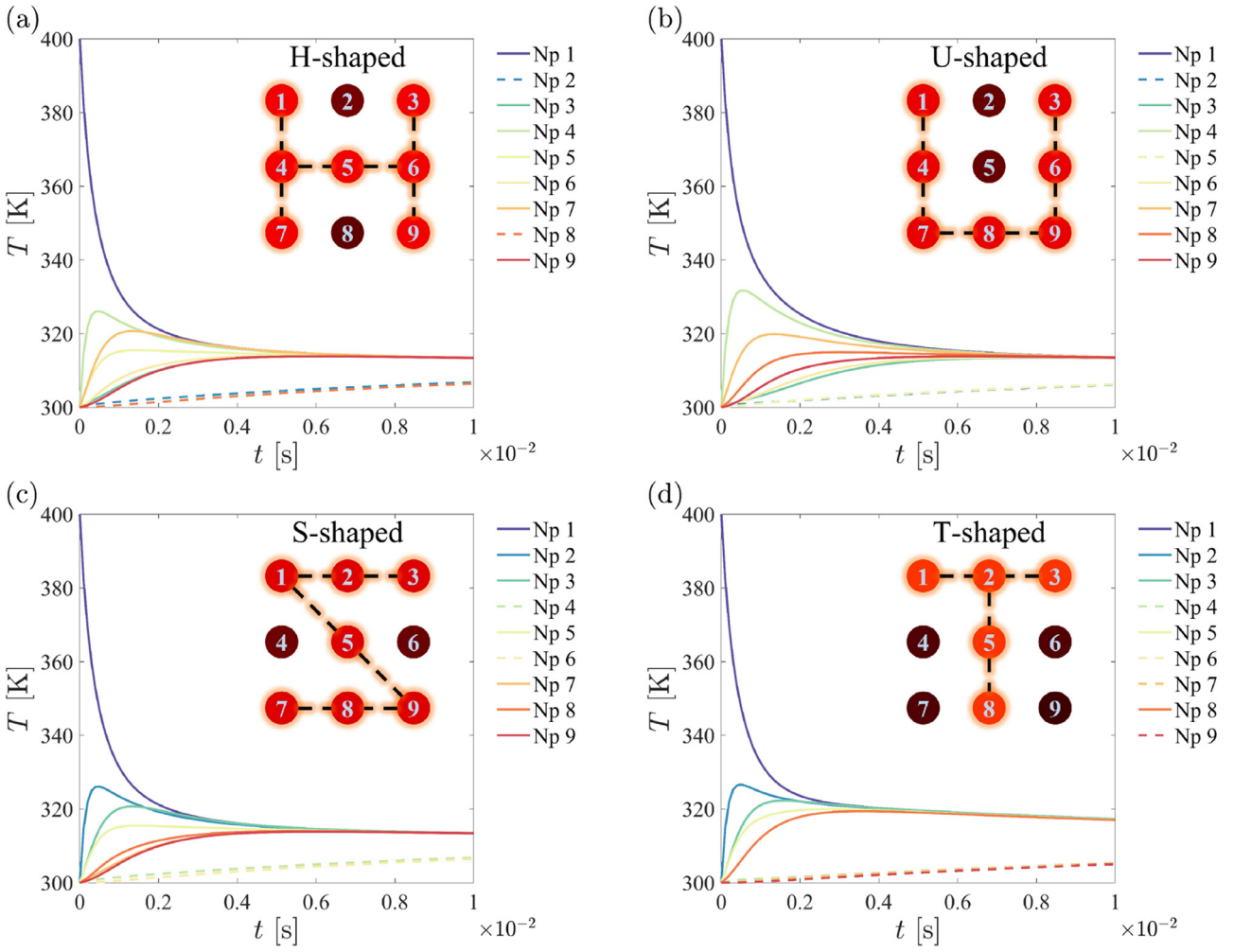

Fig. 2. Temporal evolution of temperatures of each nanoparticle (denoted by Np in figures hereafter) in the proposed system for (a) $\mu_2 = \mu_8 = 0.1$ eV, (b) $\mu_2 = \mu_5 = 0.1$ eV, (c) $\mu_4 = \mu_6 = 0.1$ eV and (d) $\mu_4 = \mu_6 = \mu_7 = \mu_9 = 0.1$ eV, with Fermi levels of the others being 0.7 eV, when particle 1 is the thermal source. All radii are 50 nm with all center-to-center distances between neighbouring particles $l = 150$ nm.

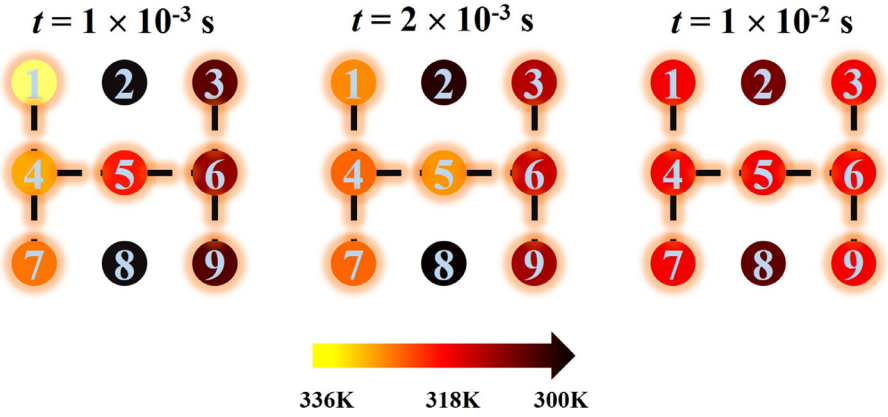

Fig. 3. Simplified pseudo-color patterns during the formation of the letter H at three time points: $t = 1 \times 10^{-3}$ s, $t = 2 \times 10^{-3}$ s and $t = 1 \times 10^{-2}$ s, respectively. (For interpretation of the references to color in this figure, the reader is referred to the web version of this article.)

nanoparticle) which is strongly dependent of Fermi level and endows GSCS nanoparticle with high tunability.

Taking the H-shaped pattern in Fig. 2(a) as an example, we investigate the thermal power of the ith particle received from all other particles, *i.e.*, $\mathcal{F}_{i,j}$ at $t = 2 \times 10^{-3}$ s, to explain how the Fermi level matching affects the heat flow, as shown in Fig. 6. At this moment, the temperature of thermal source T_1 reduces to about 321 K. In the networks, all particles radiate energy for self-cooling, so that $\mathcal{F}_i$ is always negative (not shown here). Interestingly, in accordance with the symmetry of geometry and distribution of Fermi levels, the distribution of height of each bar (radiative heating of the ith particle by others), *i.e.*, $\sum \mathcal{F}_{i,j}$, is symmetrical: $\sum \mathcal{F}_{4,j} \approx \sum \mathcal{F}_{6,j}$, $\sum \mathcal{F}_{1,j} \approx \sum \mathcal{F}_{3,j} \approx \mathcal{F}_{7,j} \approx \sum \mathcal{F}_{9,j}$ and $\sum \mathcal{F}_{2,j} \approx \sum \mathcal{F}_{8,j}$. This directly leads to that particles 2 and 8 show lower temperatures

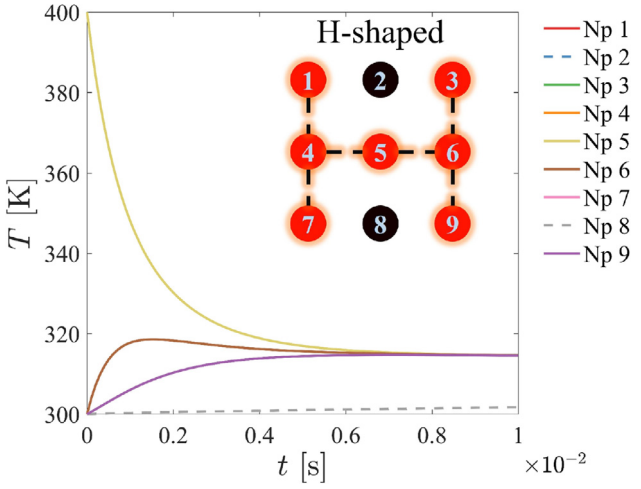

Fig. 4. Temporal evolution of temperatures of all particles in the proposed system with $\mu_2 = \mu_8 = 0.1$ eV and Fermi levels of the others being 0.7 eV, when particle 5 is the thermal source. The hotter particles and colder ones are marked in light red and black, respectively. (For interpretation of the references to color in this figure legend, the reader is referred to the web version of this article.)

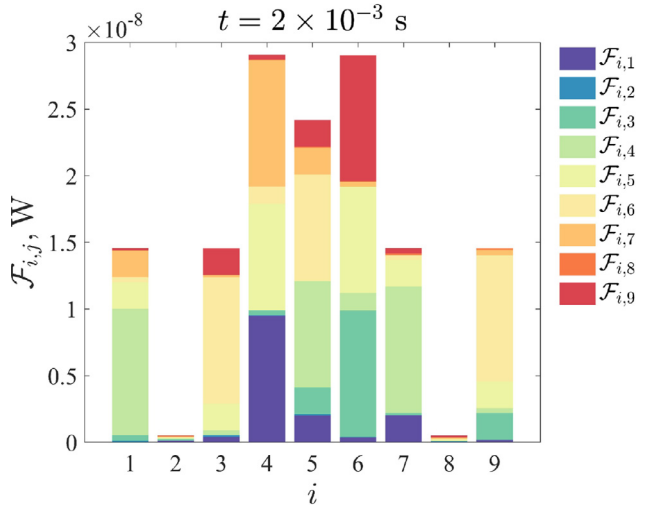

Fig. 6. Radiative heating of the ith particle by other particles $\mathcal{F}_{i,j}$. $\mu_2 = \mu_8 = 0.1$ eV with Fermi levels of the others being 0.7 eV. All radii are 50 nm with all center-to-center distances between neighbouring particles $l = 150$ nm.

than others, and gives rise to the formation of the H-shaped thermal pattern. Notice that, although particles 2-9 start at a low identical temperature (300 K), their mutual interaction also plays an important role in the thermalization process. In addition, we define the radiated energy distribution coefficient from the jth particle to the ith one ($j \neq i$), $\gamma_{j\to i} = \mathcal{F}_{i,j} / \sum_i \mathcal{F}_{i,j}$, to clearly demonstrate the heat splitting effect in the networks. We find that, taking particle 1 as a example, due to the short distance and match of Fermi levels between particles 1 and 4, particle 4 receives the most radiative heating energy from particle 1 with $\gamma_{4,1} = 65.10\%$. Particle 2 receives greatly less energy (only occupies 0.82%) than particle 4 due to the dismatch of Fermi levels despite the identical center-to-center distance. Because particle 8 is far away from particle 1 and $\mu_8 \neq \mu_1$, it receives approximately null energy from particle 1. It is noteworthy that, for the jth particle, the energy distribution coefficient $\gamma_{j\to i}$ in the system only depends on the geometry and Fermi levels of GSCS nanoparticles, and keeps unchanged with the increase of time.

We consider the effects of geometry of the system on the radiative heat transfer for the H-shaped pattern, as shown in Fig. 7. When the radii of all particles decrease to $R = 40$ nm with $l = 150$

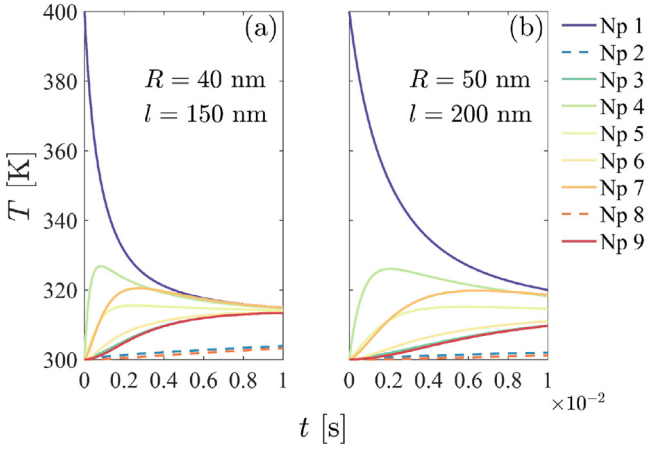

Fig. 7. Temporal evolution of temperatures of all particles in two cases: (a) $R = 40$ nm and $l = 150$ nm; (b) $R = 50$ nm and $l = 200$ nm. $\mu_2 = \mu_8 = 0.1$ eV with Fermi levels of the others being 0.7 eV, when particle 1 is the thermal source.

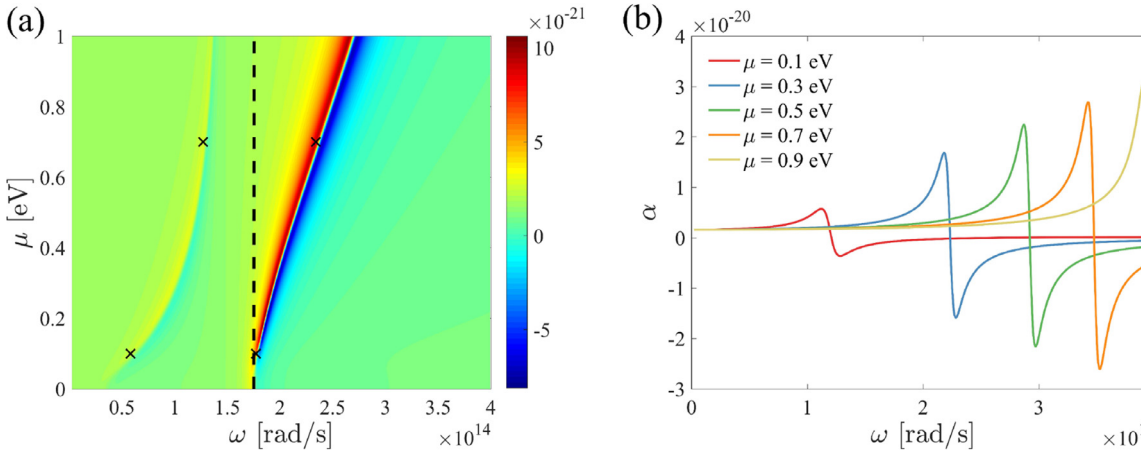

Fig. 5. (a) Polarizability dependence of a GSCS nanoparticle versus μ. The major and minor polarizability peaks for $\mu = 0.1$ and 0.7 eV are marked by x-marks. The dotted line denotes the polarizability peak of a bare SiC nanoparticle with $R = 50$ nm. (b) Polarizabilities of the bare graphene shell with $R = 50$ nm under variant Fermi levels.

nm being fixed, this system possesses a larger temperature difference with $\Delta T \approx 11$ K at $t = 1 \times 10^{-2}$ s, as shown in Fig. 7(a). Despite that smaller particles have less heat capacity which is beneficial for the temperature increase, they simultaneously result in less intense electric responses which weaken the radiative heat transfer. Obviously, the latter effect plays a more important role in the networks. When the center-center distances l increase to 200 nm with $R = 50$ nm being fixed, particles with $\mu = 0.7$ eV (the hotter ones) exhibit very different temperatures at $t = 1 \times 10^{-2}$ s, as shown in Fig. 7(b). This means that, the system shows an out-of-order temperature distribution, demonstrating the weakening of radiative heat transfer caused by a larger distance.

4. Conclusions

In summary, we have theoretically investigated the near-field radiative heat transfer in a many-body system consisting of GSCS nanoparticles. We find that, the graphene shells remarkably affect the localized surface resonance of the particle, which plays a significant role in the radiative heat transfer within the system. Consequently, according to the heat splitting effect, the controllable temperature distribution induced by the directional heat flow enables the thermal routing to be realized. This system, serving as a *module*, can also easily be generalized to a larger-scale integrated thermal device. Due to the highly tunable optical properties of graphene, this system also has great potential to actively control the heat flux. It is noteworthy that the experimental realization is indeed challenging but can still refer to some state-of-the-art measurements [56,57]. Thermal routing is a basic functionality which can be utilized for thermal management, information technology and so on. For example, design of propagation path of heat flow facilitates heat-sensitive components to avoid thermalization for maintaining their life and performance, and it can also makes system show designated infrared thermal patterns which can be decrypted by near-field thermal imaging but are encrypted in the visible light [58–60]. This work could be used to actively tune heat flow in integrated nano-objects for thermal manipulation, and also provides a guideline for exploiting novel thermal functionalities via radiative heat transfer at the nanoscale.

Declaration of Competing Interest

The authors declare that they have no known competing financial interests or personal relationships that could have appeared to influence the work reported in this paper.

CRediT authorship contribution statement

Jinlin Song: Conceptualization, Methodology, Writing - original draft. **Lu Lu:** Investigation. **Bowen Li:** Data curation. **Bo Zhang:** Visualization. **Run Hu:** Writing - review & editing. **Xinping Zhou:** Validation. **Qiang Cheng:** Supervision, Funding acquisition.

Acknowledgments

This work was mainly supported by the National Natural Science Foundation of China (51806070, 51606074 and 51676077), the Fundamental Research Funds for the Central Universities (2016YXZD009), and the China Postdoctoral Science Foundation (2018M632849).

References

[1] A. Carnicer, B. Javidi, Optical security and authentication using nanoscale and thin-film structures, Adv. Opt. Photon. 9 (2) (2017) 218–256, doi:10.1364/AOP.9.000218.

[2] B. Javidi, A. Carnicer, M. Yamaguchi, T. Nomura, E. Pérez-Cabré, M.S. Millán, N.K. Nishchal, R. Torroba, J.F. Barrera, W. He, X. Peng, A. Stern, Y. Rivenson, A. Alfalou, C. Brosseau, C. Guo, J.T. Sheridan, G. Situ, M. Naruse, T. Matsumoto, I. Juvells, E. Tajahuerce, J. Lancis, W. Chen, X. Chen, P.W.H. Pinkse, A.P. Mosk, A. Markman, Roadmap on optical security, J. Opt. UK 18 (8) (2016) 083001. http://stacks.iop.org/2040-8986/18/i=8/a=083001

[3] X. Li, Y. Xie, B. Song, H.-L. Zhang, H. Chen, H. Cai, W. Liu, Y. Tang, A stimuli-responsive smart lanthanide nanocomposite for multidimensional optical recording and encryption, Angew. Chem. Int. Ed. 56(10) 2689–2693. doi:10.1002/anie.201700011.

[4] C. Zhang, B. Wang, W. Li, S. Huang, L. Kong, Z. Li, L. Li, Conversion of invisible metal-organic frameworks to luminescent Perovskite nanocrystals for confidential information encryption and decryption, Nat. Commun. 8 (1) (2017) 1138.

[5] R. Hu, S. Zhou, Y. Li, D.-Y. Lei, X. Luo, C.-W. Qiu, Illusion thermotics, Adv. Mater. 30 (22) (2018) 1707237, doi:10.1002/adma.201707237.

[6] R. Hu, S. Huang, M. Wang, L. Zhou, X. Peng, X. Luo, Binary thermal encoding by energy shielding and harvesting units, Phys. Rev. Appl. 10 (2018) 054032, doi:10.1103/PhysRevApplied.10.054032.

[7] R. Hu, S. Huang, M. Wang, X. Luo, J. Shiomi, C.-W. Qiu, Encrypted thermal printing with regionalization transformation, Adv. Mater. 0 (0) (2019) 1807849, doi:10.1002/adma.201807849.

[8] B. Li, L. Wang, G. Casati, Negative differential thermal resistance and thermal transistor, Appl. Phys. Lett. 88 (14) (2006) 143501, doi:10.1063/1.2191730.

[9] L. Wang, B. Li, Thermal memory: a storage of phononic information, Phys. Rev. Lett. 101 (2008) 267203, doi:10.1103/PhysRevLett.101.267203.

[10] L. Wang, B. Li, Thermal logic gates: computation with phonons, Phys. Rev. Lett. 99 (2007) 177208, doi:10.1103/PhysRevLett.99.177208.

[11] P. Ben-Abdallah, S.-A. Biehs, Contactless heat flux control with photonic devices, AIP Adv. 5 (5) (2015) 053502, doi:10.1063/1.4915138.

[12] M. Planck, The theory of heat radiation, Courier Corporation, 2013.

[13] A.I. Volokitin, B.N.J. Persson, Near-field radiative heat transfer and noncontact friction, Rev. Mod. Phys. 79 (2007) 1291–1329, doi:10.1103/RevModPhys.79.1291.

[14] D. Polder, M. Van Hove, Theory of radiative heat transfer between closely spaced bodies, Phys. Rev. B 4 (10) (1971) 3303.

[15] A. Narayanaswamy, G. Chen, Surface modes for near field thermophotovoltaics, Appl. Phys. Lett. 82 (20) (2003) 3544–3546.

[16] J.B. Pendry, Radiative exchange of heat between nanostructures, J. Phys. 11 (35) (1999) 6621. http://stacks.iop.org/0953-8984/11/i=35/a=301

[17] S. Shen, A. Narayanaswamy, G. Chen, Surface phonon polaritons mediated energy transfer between nanoscale gaps, Nano Lett. 9 (8) (2009) 2909–2913.

[18] L. Lu, J. Song, K. Zhou, H. Ou, Q. Cheng, Z. Luo, Ultrafast tunable near-field radiative thermal modulator made of Ge3Sb2Te6, J. Heat Trans. T Asme 141 (7) (2019), doi:10.1115/1.4043573. 072701

[19] J. Song, L. Lu, Q. Cheng, Z. Luo, Three-body heat transfer between anisotropic magneto-dielectric hyperbolic metamaterials, J. Heat Trans. T Asme 140 (8) (2018), doi:10.1115/1.4039542. 082005

[20] P. Ben-Abdallah, S.-A. Biehs, Near-field thermal transistor, Phys. Rev. Lett. 112 (2014) 044301, doi:10.1103/PhysRevLett.112.044301.

[21] P. Ben-Abdallah, A. Belarouci, L. Frechette, S.-A. Biehs, Heat flux splitter for near-field thermal radiation, Appl. Phys. Lett. 107 (5) (2015) 053109, doi:10.1063/1.4928430.

[22] P. Ben-Abdallah, Photon thermal hall effect, Phys. Rev. Lett. 116 (2016) 084301, doi:10.1103/PhysRevLett.116.084301.

[23] S.-A. Biehs, F.S.S. Rosa, P. Ben-Abdallah, Modulation of near-field heat transfer between two gratings, Appl. Phys. Lett. 98 (24) (2011) 243102, doi:10.1063/1.3596707.

[24] L. Cui, Y. Huang, J. Wang, K.-Y. Zhu, Ultrafast modulation of near-field heat transfer with tunable metamaterials, Appl. Phys. Lett. 102 (5) (2013) 053106, doi:10.1063/1.4790292.

[25] K. Joulain, Y. Ezzahri, J. Drevillon, B. Rousseau, D.D.S. Meneses, Radiative thermal rectification between sic and SiO2, Opt. Express 23 (24) (2015) A1388–A1397, doi:10.1364/OE.23.0A1388.

[26] Y. Yang, S. Basu, L. Wang, Vacuum thermal switch made of phase transition materials considering thin film and substrate effects, J. Quant. Spectrosc. Radiat. 158 (2015) 69–77, doi:10.1016/j.jqsrt.2014.12.002.

[27] B. Zhao, J. Zhao, Z. Zhang, Enhancement of near-infrared absorption in graphene with metal gratings, Appl. Phys. Lett. 105 (3) (2014) 031905.

[28] W. Gao, J. Shu, C. Qiu, Q. Xu, Excitation of plasmonic waves in graphene by guided-mode resonances, ACS Nano 6 (9) (2012) 7806–7813.

[29] S. Thongrattanasiri, F.H. Koppens, F.J.G. De Abajo, Complete optical absorption in periodically patterned graphene, Phys. Rev. Lett. 108 (4) (2012) 047401.

[30] X. Liu, Z. Zhang, Graphene-assisted near-field radiative heat transfer between corrugated polar materials, Appl. Phys. Lett. 104 (25) (2014) 251911.

[31] P. Van Zwol, S. Thiele, C. Berger, W. De Heer, J. Chevrier, Nanoscale radiative heat flow due to surface plasmons in graphene and doped silicon, Phys. Rev. Lett. 109 (26) (2012) 264301.

[32] J. Song, Q. Cheng, Near-field radiative heat transfer between graphene and anisotropic magneto-dielectric hyperbolic metamaterials, Phys. Rev. B 94 (12) (2016) 125419.

[33] O. Ilic, N.H. Thomas, T. Christensen, M.C. Sherrott, M. Soljačić, A.J. Minnich, O.D. Miller, H.A. Atwater, Active radiative thermal switching with graphene plasmon resonators, ACS Nano 12 (3) (2018) 2474–2481.

[34] L. Wei, W. Da, G. Liwei, J. Yuping, Y. Manping, H. Jiao, L. Zhilin, P. Yuan, Y. Wenxia, C. Xiaolong, Bipolar carrier transfer channels in epitaxial graphene/sic coreshell heterojunction for efficient photocatalytic hydrogen evolution, Adv. Mater. 27 (48) (2015) 7986–7991.
[35] J.-F. Li, J.R. Anema, T. Wandlowski, Z.-Q. Tian, Dielectric shell isolated and graphene shell isolated nanoparticle enhanced raman spectroscopies and their applications, Chem. Soc. Rev. 44 (2015) 8399–8409, doi:10.1039/C5CS00501A.
[36] H.B. Chan, Y. Bao, J. Zou, R.A. Cirelli, F. Klemens, W.M. Mansfield, C.S. Pai, Measurement of the Casimir force between a gold sphere and a silicon surface with nanoscale trench arrays, Phys. Rev. Lett. 101 (2008) 030401, doi:10.1103/PhysRevLett.101.030401.
[37] A. Canaguier-Durand, P.A.M. Neto, A. Lambrecht, S. Reynaud, Thermal Casimir effect in the plane-sphere geometry, Phys. Rev. Lett. 104 (2010) 040403, doi:10.1103/PhysRevLett.104.040403.
[38] K. Chen, S. Fan, Nonequilibrium casimir force with a nonzero chemical potential for photons, Phys. Rev. Lett. 117 (2016) 267401, doi:10.1103/PhysRevLett.117.267401.
[39] R. Yu, A. Manjavacas, F.J.G. de Abajo, Ultrafast radiative heat transfer, Nat. Commun. 8 (1) (2017) 2.
[40] P. Ben-Abdallah, S.-A. Biehs, K. Joulain, Many-body radiative heat transfer theory, Phys. Rev. Lett. 107 (11) (2011) 114301.
[41] T. Christensen, A.-P. Jauho, M. Wubs, N.A. Mortensen, Localized plasmons in graphene-coated nanospheres, Phys. Rev. B 91 (12) (2015) 125414.
[42] R. Messina, M. Tschikin, S.-A. Biehs, P. Ben-Abdallah, Fluctuation-electrodynamic theory and dynamics of heat transfer in systems of multiple dipoles, Phys. Rev. B 88 (2013) 104307, doi:10.1103/PhysRevB.88.104307.
[43] M. Nikbakht, Three-body radiation dynamics in systems with anisotropic nanoparticles, EPL (Europhys. Lett.) 110 (1) (2015) 14004. http://stacks.iop.org/0295-5075/110/i=1/a=14004
[44] M. Nikbakht, Radiative heat transfer in anisotropic many-body systems: tuning and enhancement, J. Appl. Phys. 116 (9) (2014) 094307.
[45] P. Ben-Abdallah, K. Joulain, J. Drevillon, C. Le Goff, Heat transport through plasmonic interactions in closely spaced metallic nanoparticle chains, Phys. Rev. B 77 (2008) 075417, doi:10.1103/PhysRevB.77.075417.
[46] C.F. Bohren, D.R. Huffman, Absorption and Scattering of Light by Small Particles, John Wiley & Sons, 2008.
[47] J. Le Gall, M. Olivier, J.-J. Greffet, Experimental and theoretical study of reflection and coherent thermal emissionby a sic grating supporting a surface-phonon polariton, Phys. Rev. B 55 (15) (1997) 10105.
[48] L. Falkovsky, Optical properties of graphene, J. Phys. Conf. Ser. 129 (2008) 012004. IOP Publishing.
[49] S. Albaladejo, R. Gómez-Medina, L.S. Froufe-Pérez, H. Marinchio, R. Carminati, J. Torrado, G. Armelles, A. García-Martín, J.J. Saénz, Radiative corrections to the polarizability tensor of an electrically small anisotropic dielectric particle, Opt. Express 18 (4) (2010) 3556–3567.
[50] Z.-Z. Lin, C.-L. Huang, Z. Huang, W.-K. Zhen, Surface/interface influence on specific heat capacity of solid, shell and core-shell nanoparticles, Appl. Therm. Eng. 127 (2017) 884–888, doi:10.1016/j.applthermaleng.2017.08.104.
[51] O.O. Kubaschewski, C.B. Alcock, P.J. Spencer, Materials Thermochemistry, 6th revised ed., Butterworth-Heinemann Ltd., Oxford, 1993.
[52] E. Pop, V. Varshney, A.K. Roy, Thermal properties of graphene: fundamentals and applications, MRS Bull. 37 (12) (2012) 12731281, doi:10.1557/mrs.2012.203.
[53] E. Tervo, Z. Zhang, B. Cola, Collective near-field thermal emission from polaritonic nanoparticle arrays, Phys. Rev. Mater. 1 (2017) 015201, doi:10.1103/PhysRevMaterials.1.015201.
[54] J. Dong, J. Zhao, L. Liu, Radiative heat transfer in many-body systems: coupled electric and magnetic dipole approach, Phys. Rev. B 95 (2017) 125411, doi:10.1103/PhysRevB.95.125411.
[55] J. Song, Q. Cheng, Z. Luo, X. Zhou, Z. Zhang, Modulation and splitting of three-body radiative heat flux via graphene/sic core-shell nanoparticles, Int. J. Heat Mass Transf. 140 (2019) 80–87, doi:10.1016/j.ijheatmasstransfer.2019.05.102.
[56] K. Kim, B. Song, V. Fernández-Hurtado, W. Lee, W. Jeong, L. Cui, D. Thompson, J. Feist, M.T.H. Reid, F.J. García-Vidal, J.C. Cuevas, E. Meyhofer, P. Reddy, Radiative heat transfer in the extreme near field, Nature 528 (2015) 387.
[57] L. Cui, W. Jeong, V. Fernández-Hurtado, J. Feist, F.J. García-Vidal, J.C. Cuevas, E. Meyhofer, P. Reddy, Study of radiative heat transfer in Ångström- and nanometre-sized gaps, Nat. Commun. 8 (2017) 14479.
[58] Y. De Wilde, F. Formanek, R. Carminati, B. Gralak, P.-A. Lemoine, K. Joulain, J.-P. Mulet, Y. Chen, J.-J. Greffet, Thermal radiation scanning tunnelling microscopy, Nature 444 (7120) (2006) 740–743.
[59] G. Baffou, P. Bon, J. Savatier, J. Polleux, M. Zhu, M. Merlin, H. Rigneault, S. Monneret, Thermal imaging of nanostructures by quantitative optical phase analysis, ACS Nano 6 (3) (2012) 2452–2458, doi:10.1021/nn2047586. PMID: 22305011.
[60] G. Bakan, S. Ayas, M. Serhatlioglu, C. Elbuken, A. Dana, Invisible thin-film patterns with strong infrared emission as an optical security feature, Adv. Opt. Mater. 0(0) 1800613. doi:10.1002/adom.201800613.